View metadata, citation and similar papers at core.ac.uk

brought to you by CORE

provided by Queen Mary Research Online

energy&fuels

Queen Mary University of London | Library Services

Subscriber access provided by Queen Mary, University of London

Fossil Fuels

Application of a Digital Oil Model to Solvent-Based Enhanced Oil Recovery of Heavy Crude Oil

Motoaki Iwase, Yunfeng Liang, Yoshihiro Masuda, Masato Morimoto, Toshifumi Matsuoka, Edo S. Boek, Yutaro Kaito, and Kazunori Nakagawa

Energy Fuels, **Just Accepted Manuscript** • DOI: 10.1021/acs.energyfuels.9b02801 • Publication Date (Web): 17 Oct 2019

Downloaded from pubs.acs.org on October 30, 2019

Just Accepted

"Just Accepted" manuscripts have been peer-reviewed and accepted for publication. They are posted online prior to technical editing, formatting for publication and author proofing. The American Chemical Society provides "Just Accepted" as a service to the research community to expedite the dissemination of scientific material as soon as possible after acceptance. "Just Accepted" manuscripts appear in full in PDF format accompanied by an HTML abstract. "Just Accepted" manuscripts have been fully peer reviewed, but should not be considered the official version of record. They are citable by the Digital Object Identifier (DOI®). "Just Accepted" is an optional service offered to authors. Therefore, the "Just Accepted" Web site may not include all articles that will be published in the journal. After a manuscript is technically edited and formatted, it will be removed from the "Just Accepted" Web site and published as an ASAP article. Note that technical editing may introduce minor changes to the manuscript text and/or graphics which could affect content, and all legal disclaimers and ethical guidelines that apply to the journal pertain. ACS cannot be held responsible for errors or consequences arising from the use of information contained in these "Just Accepted" manuscripts.

is published by the American Chemical Society. 1155 Sixteenth Street N.W., Washington, DC 20036

Published by American Chemical Society. Copyright © American Chemical Society. However, no copyright claim is made to original U.S. Government works, or works produced by employees of any Commonwealth realm Crown government in the course of their duties.

Application of a Digital Oil Model to Solvent-Based Enhanced Oil Recovery of Heavy Crude Oil

Motoaki Iwase[1], Yunfeng Liang[,1], Yoshihiro Masuda*[,1], Masato Morimoto[2], Toshifumi Matsuoka[3], Edo S. Boek[4], Yutaro Kaito[5], and Kazunori Nakagawa[5]*

[1]*Department of Systems Innovation, The University of Tokyo, Tokyo 113-8656, Japan*

[2]*National Institute of Advanced Industrial Science and Technology (AIST), Ibaraki 305-8569, Japan*

[3]*Fukada Geological Institute, Tokyo 113-0021, Japan*

[4]*Division of Chemical Engineering & Renewable Energy, School of Engineering and Materials Science, Queen Mary University of London, London E1 4NS, United Kingdom*

[5]*Japan Petroleum Exploration Co., Ltd. (JAPEX), Chiba 261-0025, Japan*

ABSTRACT: To investigate enhanced oil recovery processes, we constructed a molecular model of a live heavy crude oil (digital oil) and studied the crude oil properties at the reservoir temperature and a wide range of pressures. We identified the liquid phase components of the digital oil by flash calculation, and calculated the density and viscosity by molecular dynamics simulations. The calculated density and viscosity were in good agreement with experimental data. To evaluate the effectiveness of various solvents to enhance oil recovery, we calculated the oil property changes when different solvents were added to the digital oil. First, we compared methane and carbon dioxide (CO_2). The results indicated that CO_2 was more effective in terms of oil-viscosity reduction, oil swelling, and diffusion in the oil. Second, we evaluated the effectiveness of 11 different solvents: nitrogen, CO_2, methane, ethane, propane, *n*-heptane, *n*-octane, toluene, and three xylene isomers (*o*-xylene, *m*-xylene, and *p*-xylene). Ethane had the greatest effect on oil-viscosity reduction and oil swelling, and CO_2 had the highest diffusion coefficient. From these results, ethane and CO_2 are appropriate solvents for this crude oil. In addition, it is interesting to note that the decreases of the viscosity among the three xylene isomers were different, but there were no differences in the swelling factors and diffusion coefficients. The different rotation motion characteristics of the xylene isomers can account for the viscosity differences. Such information will be helpful for further development of digital oil models.

1. INTRODUCTION

Efficient recovery of heavy oil, which includes extra heavy oil and bitumen, is important with the depletion of conventional light oil reserves and the increase of energy demands. The main difficulty in heavy oil recovery is that heavy oil is partially or completely immobile under reservoir conditions because of its extremely high viscosity and heavy molecular composition.[1–4] Enhanced oil recovery (EOR) is therefore an essential technique for heavy-oil recovery, even at the early development stage. Steam-assisted gravity drainage (SAGD) is the most widely commercialized process for bitumen and heavy-oil recovery.[5–7] SAGD takes advantages of the strong temperature dependency of the bitumen viscosity. The role of steam injection is to provide heat and reduce the viscosity of the heavy oil to enable it to move toward the production well. In the SAGD process, the steam injected from a horizontal well forms a steam chamber. Under gravity, the heated bitumen drains toward the production well, which is located a few meters below the injection well.[7] This process offers several key advantages, including high ultimate recovery and a stable oil production rate. However, high energy demands and environmental concerns, such as high carbon dioxide (CO_2) emission levels and the use of large quantities of fresh water, have prompted the need for alternative processes.[5–7]

Solvent-aided SAGD (SA-SAGD) has been proposed as an alternative to improve the efficiency of SAGD.[5–9] In SA-SAGD, a small amount of a hydrocarbon solvent is co-injected with water steam to further reduce the viscosity of the bitumen near the chamber edge. This process requires a smaller amount of steam (i.e., less consumption of energy and water) to recover the same amount of bitumen and can exhibit a higher oil production rate than SAGD.[6,9] Vapor extraction (VAPEX), a cold-production process, has also been proposed as an alternative for heavy-oil recovery.[10–13] In VAPEX, vaporized solvents are injected instead of steam, which dissolve in the oil, dilute the oil,

and decrease its viscosity. Compared with liquid solvents, vaporized solvents provide a higher driving force for gravity drainage of heavy oil and are more easily recoverable.[12]

In both SA-SAGD and VAPEX processes, selecting an appropriate solvent for a particular reservoir is the most important task because the solvent effectiveness varies depending on the oil field.[5–7,12,13] For example, the majority of VAPEX studies have used propane as the injected solvent because propane is one of the least-expensive hydrocarbon solvents and it has satisfactory solubility in heavy oil.[12] CO_2 has also attracted attention as the solvent. CO_2 is more soluble in heavy oil than propane, so it can more significantly decrease the oil viscosity.[13] In addition, it decreases the cost of the injected solvent because CO_2 can be recovered from the exhaust and by-product gases.[13]

The oil viscosity is an important factor for evaluating the effectiveness of different solvents.[2,10,11] For heavy oils, characterizing the viscosity behavior is particularly important because even a small change can have large effects on the production rate and recoverable oil volume.[2] The production rates of SA-SAGD and VAPEX are also strongly dependent on the oil viscosity reduction, which in turn depends on dissolution of the solvent in the heavy oil, mainly by molecular diffusion.[11,14] Therefore, the diffusion coefficient of the solvent is another important factor. Molecular diffusion is caused by the concentration gradients of each component in the oil and gas phases. This diffusion effect is especially important in the gas injection process because concentration gradients easily occur near the injection zone in this process. The molecular diffusion coefficients in oils have been characterized in several ways.[8,15,16] Ohata et al.[15] estimated the molecular diffusion coefficients from a combination of experimental data using a pressure–volume–temperature (PVT) cell and simulation matching to the pressure decay. Imai et al.[8] estimated the molecular diffusion coefficients by reproducing the time-lapse concentration profiles

obtained by X-ray computed tomography imaging. The swelling factor, which is defined as the ratio of the volume of the oil–solvent mixture to the original oil volume, is also an important parameter. Oil swelling is expansion of the oil volume when a solvent contacts the reservoir fluid, which can result in enhancement of oil recovery by mobilizing the residual oil and increasing the oil saturation and relative permeability.[13,17] Understanding these properties leads to selection of an effective solvent, field design of the recovery processes, and understanding the oil-recovery mechanisms. These properties are determined based on the interactions between the oil components and the solvent. It is therefore necessary to understand the oil components and the changes in their properties when various solvents are added.

Owing to the development of computational technology, molecular dynamics (MD) simulations are now widely used to investigate oil–water interfacial phenomena,[18–23] petroleum engineering,[20–26] oil refinery,[27] and asphalt systems.[28–30] Molecular models are being developed for asphaltenes,[31,32] as well as whole crude oil.[33,34] One of the advantages of MD simulations is that they provide insights that cannot be extracted from experimental data alone. In our previous work, we constructed a digital oil model (i.e., a molecular model of crude oil) for a light crude oil,[33] as well as another digital oil model for a heavy crude oil.[34] We also showed the potential application of digital oil to asphaltene precipitation prediction.[33] In this study, we applied the digital oil model to investigate the solvent-based EOR processes of a heavy crude oil.

2. METHODOLOGY

2.1. Overview

For MD simulations, it is important to construct an accurate molecular model of crude oil. Theoretically, a molecular model of crude oil must contain all of the components of that oil. However, it is not possible to detect all of these components, especially for a heavy crude oil. Thus, the molecular model needs to be appropriately simplified. One approach to characterize a complex mixture is to use average data based on measurements of the whole sample.[31,32] Digital oil is a molecular model of crude oil that is represented as a mixture of the representative molecules of each fraction.[33,34] Because the representative molecules are generated on the basis of the average structural information of that fraction, all of the components do not need to be identified (when separation is unworkable). Once we construct a digital oil, we can analyze both its macroscopic properties and microscopic phenomena under any thermodynamic conditions by MD simulations.

A schematic diagram of the EOR study with the digital oil model is shown in **Figure 1**. In this study, we used a heavy crude oil as an example. The American Petroleum Institute (API) gravity of the crude oil was 11°–17°. The density of our sample at ambient pressure and 288 K was 0.955 g/cm^3. In our previous work, we constructed a digital oil model (dead oil model) for this heavy crude oil and calculated its physical properties.[34] In this study, we first constructed a live oil model that contained both dead oil and dissolved gas components. We then calculated the density and viscosity at the reservoir temperature and a wide range of pressures by MD simulations and compared the results with the experimental data for validation. After confirming the validity of the model, we calculated the changes in the oil properties when various solvents were added to the digital oil. We finally evaluated the effectiveness of the solvents in terms of oil-viscosity

reduction, oil swelling, and solvent diffusion in the oil. We give a brief summary of construction and validation of the digital oil model in Section 2.2. We explain the MD simulation details in Section 2.3. We discuss identification of the liquid phase components in Section 2.4. We describe our experiments on measuring the crude oil properties of a crude oil (density and viscosity) and the changes in the properties when adding natural gas (methane) and CO_2 in Section 2.5.

2.2. Construction of the Digital Oil Model

A schematic diagram of the procedure to construct a digital oil model for a heavy crude oil is shown in **Figure 2**. It differs from the procedure to construct a digital oil model for a light crude oil because we could not identify all of the molecular structures and their mole fractions of the light fractions, such as saturates and aromatics, in the heavy crude oil by gas chromatography–mass spectrometry and gas chromatography with flame ionization detection.[33]

For the heavy crude oil, the crude oil was separated into four fractions: saturates, aromatics, resins, and asphaltenes (SARA). First, it was diluted with heptane and separated into the precipitated asphaltenes and the dissolved maltenes in heptane by filtration and refluxing.[34] The saturates, aromatics, and resins were then extracted from the maltenes by using an alumina column with heptane, toluene, and methanol–toluene solvents. The yields of the SARA fractions for the investigated heavy crude oil are given in **Table 1**. The digital oil model was constructed as a mixture of the representative molecules of saturates, aromatics, resins, and asphaltenes. The lost components (low boiling-point compounds vaporized during drying) were determined based on gas chromatography distillation (GCD) experiments.[34] In this specific case, asphaltenes of ~0.4 wt % in the crude oil were ignored.[34] The representative molecules were generated by quantitative molecular representation (QMR),[32] a technique that provides a set of molecules consistent with the

analytical data, such as the elemental composition, the average molecular mass, and the structural types of hydrogen and carbon atoms revealed by ^{1}H and ^{13}C NMR spectroscopy. To enable the QMR method to be applicable to saturates, we made two developments: (1) nonaromatic molecules could be generated by a new algorithm, which can also generate more branched structures, and (2) the molecular mass distribution of the model could be fitted to that obtained from experiments. The thus obtained digital oil model was composed of 36 types of representative molecules. We validated the model in terms of the double-bond equivalent as a function of the carbon number. We also confirmed the validity of the model by comparison with the experimental density and viscosity.[34]

Crude oil under the reservoir conditions (i.e., live oil) is composed of oil components (dead oil) and dissolved gas components. Here, dead oil means a crude oil that does not contain any dissolved gas. It is usually a sample at ambient pressure, so the oil has lost its volatile components. Live oil means a crude oil containing dissolved gas in solution. It is usually a sample taken from a reservoir (e.g., a bottom-hole sample) without loss of the dissolved gas that can be released from the solution when the pressure is lower than the bubble point pressure. In our previous work,[34] we focused on a digital oil model containing only dead oil. The live oil properties under reservoir conditions need to be calculated to simulate the EOR processes. Hence, we constructed a live oil model by adding gas components to the dead oil model. A snapshot of the digital oil model is shown in **Figure 3**. The proportions of the gas components in the live oil obtained from experiments are given in **Table 2**. Based on these results, the number of molecules of each gas component in the live oil model was determined (also given in **Table 2**). The major component of the dissolved gas was the C_1 component (CH_4), followed by N_2, while the CO_2, C_2, and C_3 components were ignored in the model because of their low concentrations.

2.3. MD Simulations

We calculated the physical properties of the digital oil by MD simulations using the GROMACS package (version 5.1.4).[35] The CHARMM general force field (CGenFF) was used to describe the inter- and intramolecular interactions of the hydrocarbons, including those with heteroatoms.[36–39] In previous studies, it has been shown that the CGenFF (and the CHARMM force field) can reproduce the densities of organic liquids and interfacial tension of oil–water interfaces very well with deviation of less than 1% and 3%, respectively.[21,36,40] For CO_2 and nitrogen (N_2), the transferable potentials for phase equilibria (TraPPE) force field was used.[41] The cutoff distances were 1.2 nm for both the Lennard-Jones and electrostatic potentials. The Verlet cut-off scheme was used, where a pair list is created with a Verlet buffer at neighbor search steps.[42] The particle mesh Ewald summation method was used for the long-range electrostatic interactions.[43] To remove excess potential energy, we performed an energy minimization step using the steepest descent method. We then performed an isothermal–isobaric (NPT) ensemble simulation using the velocity-rescaling thermostat[44] and Berendsen barostat[45] until the system reached equilibrium. The density was then calculated by an NPT simulation with the Nosé–Hoover thermostat[46,47] and Parrinello–Rahman barostat[48] for 3 ns. The shear viscosity was calculated by equilibrium MD (EMD) simulations with the canonical (NVT) ensemble with the Nosé–Hoover thermostat for 5–20 ns. In contrast to the non-equilibrium MD (NEMD) method, the EMD method does not require additional adjustments of the shear rate, which enables zero-shear viscosity with comparable accuracy and reliability to the NEMD method to be obtained.[49] The details can be found in our previous studies.[33,34] The diffusion coefficients of the solvents were also calculated with the same trajectory as the viscosity calculation. The temperature was controlled at the reservoir temperature of 323.15 K and the pressure ranged from 24.2 to 0.48 MPa.

2.4. Identification of the Liquid Phase Components

The bubble point is the pressure and temperature at which the first bubble of gas comes out of the solution in oil. When the pressure is decreased below the bubble point pressure, the crude oil separates into the gas and liquid phases. In experiments, the physical properties of the liquid phase are measured below the bubble point pressure. However, in our MD simulations, phase separation could not be observed owing to size limitation.[33] There are several options to overcome this problem. The first option is to use an extraordinarily large system to clearly observe the vapor and liquid phases.[22] To this end, a coarse-grained force field[24] may be helpful to save computational cost. The second option is to perform a Gibbs ensemble Monte Carlo (GEMC) simulation, which allows two simulation boxes for the liquid and vapor phases. However, GEMC requires high computational cost, especially for large systems like our case. The third option is to perform a phase equilibrium calculation, namely, a flash calculation, which is widely used in the petroleum industry because of its low calculation cost. In this study, we performed a flash calculation using a PVT simulator (PVTsim Nova 4.0, Calsep, Kongens Lyngby, Denmark). In the PVT simulator, the PVT model was composed of heavy components and dissolved gas. The heavy components consisted of heavy hydrocarbons with carbon numbers of seven or more (C_{7+}), while the dissolved gas consisted of CO_2, N_2, and light hydrocarbons (C_1–C_3). In the flash calculation of the crude oil, 17 types of pseudocomponents were used (12 heavy components and 5 dissolved gas components). When we constructed the cubic equation of state (EoS) model, we modeled the pseudocomponents based on the Pedersen approach.[50] In this approach, the critical temperature, critical pressure, and acentric factor of each component were estimated by the correlation proposed by Pedersen et al.,[50] that is, the effect of the naphthenic and aromatic components in each pseudocomponent was included through the density and molecular weight.[50] We used the Peng–Robinson EoS. The EoS

model was adjusted to match the PVT experimental data. From the flash calculation, we obtained the proportions of each component in both the gas and liquid phases. The liquid component of the digital oil was then reconstructed based on the results of the flash calculation. Similarly, we determined the liquid components by flash calculations of digital oil–solvent mixtures for solvents such as CO_2, N_2, methane, ethane, and propane.

2.5. Measurement of the Crude Oil Properties

We measured the physical properties (density and viscosity) of the crude oil (a live oil) at the reservoir temperature (323.15 K) and a wide range of pressures (24.2–0.48 MPa) using a PVT cell.[15] In the PVT experimental system, the temperature was maintained using a thermostat. A free piston separated the oil sample and silicon oil, which controls the pressure. The interface level between the liquid and vapor phases was determined by a charge coupled device camera and a high-resolution cathetometer, which can resolve the changes at the 0.01 mm level. The experimental system included a densimeter and a viscometer to measure the density and viscosity of the liquid phase. Natural gas (methane) and CO_2 were considered as the first two candidate solvents (for EOR applications) because they can be easily obtained in oil fields. When adding a solvent, the density and viscosity were measured in the same way. The largest injection amount of solvent was predetermined by referring to the reservoir pressure (~17 MPa). For methane and CO_2, they were 18.0 mol % (1.74 wt %) and 53.4 mol % (19.3 wt %) of the crude oil, respectively. These experimental data were used for comparison with the calculated data.

3. RESULTS AND DISCUSSION

3.1. Physical Properties of the Live Oil Model

To validate the live oil model, we calculated the oil density at the reservoir temperature (325.15 K) and a wide range of pressures (24.2 to 0.48 MPa). The calculated density as a function of pressure (dotted line) in comparison with the experimental data is shown in **Figure 4**. These values were in good agreement in the high-pressure range (≥10.4 MPa), but not in the low-pressure range (<10.4 MPa). This indicates that phase separation could not be observed at the spatial and time scale used in the MD simulations, which leads to calculating the total density of the gas and liquid phases. To identify the liquid phase components at each pressure, we performed flash calculations using the PVT simulator. The composition of the liquid phase at each pressure obtained from a flash calculation is given in **Table 3**. All of the heavy components (C_{7+}) were still in the liquid phase even below the bubble point pressure, while the dissolved gas components vaporized as the pressure decreased. We then reconstructed a digital oil model that contained only the liquid phase components and calculated its density at various pressures (solid line, **Figure 4**). The densities were in good agreement with the experimental values at all of the pressures (deviation <2%).

We also calculated the viscosity of the digital oil and compared it with experimental data. A comparison of the calculated and measured viscosities is shown in **Figure 5**. The calculated viscosity of the full components of the digital oil (dotted line) monotonically decreased with decreasing pressure, while the measured viscosities (open symbols) increased below the bubble point pressure. However, the calculated viscosity of the liquid phase (solid line) showed a similar trend to the measured viscosity. Like a previous study of dead oil,[34] the deviation from the measured viscosity was systematic with the calculated value being ~1.5 higher than the

experimental value. From these results, combining digital oil and flash calculation enables the physical properties of the liquid phase to be calculated, thereby confirming the validity of the live oil model in terms of the density and viscosity under the reservoir conditions.

3.2. Case Study 1: Comparison of CH_4 and CO_2

We performed two case studies using the live oil model to investigate the effective EOR processes. In case study 1, we evaluated the effectiveness of natural gas (CH_4) and CO_2 as injected solvents. These two solvents are considered to be promising candidates to enhance the recovery of this crude oil. The solvents were added to the digital oil up to their solubility limits. The injected CH_4 and CO_2 corresponded to 18.0 mol % (1.74 wt %) and 53.4 mol % (19.3 wt %) of the digital oil, respectively. The amount of injected CO_2 was about three times higher than that of CH_4 because CO_2 has higher solubility in the oil. The compositions of the liquid phases at each pressure in the cases of CH_4 and CO_2 injection are given in **Tables 4** and **5**, respectively. Based on these results, we constructed digital oil–solvent mixtures. We then evaluated the effectiveness of each solvent by calculating the viscosity and swelling factor of the digital oil with the digital oil–solvent mixtures, and the diffusion coefficient of each solvent in the digital oil.

3.2.1. Viscosity Comparison. The viscosities of the digital oil alone, digital oil–CH_4 mixture, and digital oil–CO_2 mixture in comparison with the experimentally measured values are shown in **Figure 6**. Like the calculated results for the crude oils (i.e., both live oil and dead oil),[34] the deviation was systematic with the calculated value being ~1.5 higher than the experimental value. CO_2 decreased the oil viscosity more significantly than CH_4. In addition, CH_4 decreased the oil viscosity only in the high-pressure range (≥11.8 MPa), while CO_2 decreased the oil viscosity at all of the pressures. We also confirmed that addition of solvents caused the bubble point pressures to

increase. From all of the results, CO_2 has a greater influence on EOR in terms of oil-viscosity reduction.

3.2.2. Oil Swelling Comparison. The swelling factors of the digital oil by CH_4 and CO_2 in comparison with the experimentally measured values are shown in **Figure 7**. The swelling factor in this study was calculated as the ratio of the volume of the oil–solvent mixture to the original oil volume (at 0.48 MPa). The calculated swelling factors were in good agreement with the experimental values for both CH_4 and CO_2. We confirmed that the swelling factors did not increase above the bubble point pressures. CO_2 swelled the oil by ~21%, while CH_4 swelled it by ~5% at each bubble point pressure. This also indicates that CO_2 has a greater influence on EOR in terms of oil swelling.

3.2.3. Diffusion Coefficient Comparison. The calculated diffusion coefficients of CH_4 and CO_2 in the digital oil are shown in **Figure 8**. The diffusion coefficients of both solvents increased with increasing pressure, while they slightly decreased when the pressure exceeded the bubble point pressures of ~20 MPa. The diffusion coefficient of CO_2 was about twice that of CH_4, which indicates that CO_2 can more easily diffuse in the heavy oil compared with CH_4. Therefore, it can be concluded that CO_2 is more suitable as the solvent for EOR in terms of diffusion in the oil. We did not have measured diffusion coefficient data for the same crude oil, but data was available for a crude oil from the same oil field. The density of that sample at ambient pressure and 288 K was 0.988 g/cm^3. The measurement was at 17 MPa and 323 K. Our calculated data were in agreement with the measured data[15] in terms of the order of magnitude (~10^{-9} m^2/s) and the fact that the diffusion coefficient of CO_2 was larger than that of CH_4.

Consequently, CO_2 is an effective solvent in terms of oil-viscosity reduction, oil swelling, and diffusion in the oil. This is mainly because CO_2 has high solubility in the heavy oil, which results in a large number of molecules added to the digital oil. We thus found that the solubility of the solvent has a great influence on EOR.

3.3. Case Study 2: Investigation of Effective Solvents

In case study 2, we investigated the solvents by evaluating the oil property changes when various solvents were added to the digital oil. The candidate solvents were N_2, CO_2, methane (CH_4), ethane, propane, *n*-heptane, *n*-octane, toluene, and the three isomers of xylene (*o*-xylene, *m*-xylene, and *p*-xylene). All of the solvents were added to the digital oil at 10 wt %. The number of molecules of each solvent was calculated according to each molecular mass (**Table 6**). Note that the solubility limits of N_2 and methane were less than 10 wt %, that is, the vapor phases emerged when these two solvents were added at 10 wt %. We therefore identified the liquid phase components of the digital oil–N_2 and digital oil–methane mixtures by flash calculation (**Table 7**). The properties evaluated were the viscosity, swelling factor, and diffusion coefficient of the solvent. The pressure and temperature were controlled at 17.0 MPa and 323.15 K, respectively, which were the same as the reservoir conditions.

3.3.1. Viscosity Comparison. A comparison of the calculated viscosities of the digital oil–solvent mixtures is shown in **Figure 9**. Ethane decreased the oil viscosity the most. CO_2 and propane also significantly decreased the oil viscosity, while the liquid solvents, including heavier alkanes (*n*-heptane and *n*-octane) and aromatics (toluene and xylene), only slightly decreased the oil viscosity. N_2 actually increased the oil viscosity. In the digital oil, the numbers of N_2 and methane molecules in the simulation system were 13 and 279, respectively (**Table 2**). However,

when N_2 was injected into the crude oil, the numbers of N_2 and methane molecules in the simulation system became 122 and 81, respectively (**Table 7**). This large relative change of the molecule numbers should account for the increase in the viscosity. Interestingly, the decreases in the viscosity were different among the three isomers of xylene. This indicates that the isomers have different influences on the oil viscosity.

3.3.2. Oil Swelling Comparison. A comparison of the swelling factors of the digital oil by different solvents is shown in **Figure 10**. Ethane swelled the oil the most, followed by propane, *n*-heptane, and *n*-octane. Methane only slightly swelled the oil and N_2 did not swell the oil. In fact, the oil shrank when injecting N_2. This is in good accordance with the above findings of the viscosity changes, where an increase of the viscosity was observed. In addition, no differences were observed between the three isomers of xylene in terms of the swelling factors.

3.3.3. Diffusion Coefficient Comparison. A comparison of the diffusion coefficients of the solvents in the digital oil is shown in **Figure 11**. CO_2 had the highest diffusion coefficient in the digital oil. Ethane also had a high diffusion coefficient. Liquid solvents, including heavier alkanes (*n*-heptane and *n*-octane) and aromatics (toluene and xylene), showed much lower diffusion coefficients. In addition, no significant differences were observed among the three isomers of xylene in terms of the diffusion coefficients.

3.4. Discussion

3.4.1. Implications for EOR Applications. In this study, a heavy crude oil sample was used as a target oil to study the EOR processes. In this oil field, there are two different reservoirs: “shallow” and “deep” reservoirs. The heavy crude oil used in this study was obtained from the shallow reservoir. The deep reservoir is a gas condensate reservoir. This oil field has not yet been in

production, so several EOR processes are now being extensively studied by experiments and simulations. Natural gas (methane) injection is considered to be a candidate (for EOR applications) because it can be easily recovered from the deep reservoir. In addition, this oil field is located near a carbon dioxide capture and storage site, so CO_2 injection is also a promising candidate. Therefore, first, we compared methane and CO_2 by calculating the oil property changes when methane or CO_2 was added to the digital oil. The results indicated that CO_2 was more effective in terms of oil-viscosity reduction, oil swelling, and diffusion in the oil. Furthermore, we evaluated the effectiveness of 11 different solvents. Ethane had the greatest influence on oil-viscosity reduction and oil swelling, and CO_2 had the highest diffusion coefficient. From these results, ethane and CO_2 are appropriate solvents for this crude oil. This indicates that vaporized solvents have advantages for recovery of heavy oil compared with liquid solvents.[12]

3.4.2. Importance of the Solubility for Vaporized Solvents. Here, we will discuss the importance of the solubility of the solvent for enhancement of oil recovery. In case study 1, the number of CO_2 molecules added to the digital oil was about five times more than that of methane molecules, which resulted in the high effectiveness of CO_2. In case study 2, the results showed that lighter normal alkanes were more effective. However, methane did not show high effectiveness, even though it is the lightest normal alkane. The difference between methane and the other normal alkanes was that the vapor phase emerged when 10 wt % methane was added to the digital oil owing to its low solubility (1.74 wt %). This indicates that solvents, especially vaporized solvents, require satisfactory solubility for high effectiveness in enhancing EOR. Consequently, from case studies 1 and 2, the solubility of the solvent is an essential factor for investigation of the effective EOR processes. This is the reason why ethane and CO_2 showed great influences on EOR.

3.4.3. Mechanisms of the Effect of the Xylene Isomers on the Viscosity: Role of the Rotational Relaxation Time. To investigate the relationship between the xylene isomers and the viscosity, we calculated the rotational correlation functions of the xylene isomers in the digital oil. Two different vectors were chosen: the normal vector of the aromatic plane and the vector from the A atom to the B atom, which are defined in **Figure 12(a)**. The reorientation correlation time was calculated by the time correlation function: $\mathrm{C}(t) =< \mathbf{u}(t) \cdot \mathbf{u}(0) >$, where **u** is the vector that is considered. Following Zhang and Greenfield,[28] we regressed the calculated results using the modified Kohlrausch–Williams–Watts function:[51] $P_{mKWW} = \alpha \exp(-t/\tau_0) + (1 - \alpha)\exp(-(t/\tau_{KWW})^{\beta})$. The time correlation functions of the normal vector of the aromatic plane and the A–B vector in the aromatic plane, and the corresponding regression curves are shown in **Figure 12(b)** and **(c)**. The rotational relaxation times (τ_C) and regression results using the modified Kohlrausch–Williams–Watts function are given in **Table 8**. It is interesting to note that the τ_C value of the normal vector of the aromatic plane of *o*-xylene is the largest, which corresponds well with it having the highest viscosity among the isomers. However, the values for *m*-xylene and *p*-xylene show the opposite trend to the calculated viscosities. This contradiction can be solved by considering the A–B vector, as shown in **Figure 12**. In this case, because the moment of inertia of *p*-xylene is higher than that of *m*-xylene, the rotational relaxation time of *p*-xylene is higher than that of *m*-xylene. Differing from Zhang and Greenfield,[28] it is still difficult to unify the picture and predict the viscosity with all of the calculated rotational relaxation times, because the comparison here was made based on different molecules, whereas it was the same molecule at different temperatures in their study. This information, that is, there is a significant influence of isomers on the viscosity, can be used for further development of the digital oil model. In most cases, isomers, like the xylene isomers, may not be distinguishable from each other in terms of the structural

parameters determined by NMR spectroscopy. Therefore, if we consider a variety of isomers for the representative molecules, the viscosity of the digital oil could change while maintaining the structural parameters.

4. CONCLUSION

To investigate the effectiveness of solvents for enhancing the EOR processes, we constructed a digital oil model of a live oil that consisted of the dead oil and dissolved gas components. The digital oil model of the dead oil was from our previous work.[34] We identified the liquid phase components of the digital oil at several pressures by flash calculation and calculated the density and viscosity of the liquid phase. The calculated properties were in good agreement with the experimental data. We then evaluated the oil property changes when different solvents were added to the oil. The main results and recommendations are as follows: (1) Vaporized solvents showed advantages for recovery of heavy oil compared with liquid solvents in terms of oil-viscosity reduction, oil swelling, and diffusion in the oil. (2) Ethane had the greatest influence on oil-viscosity reduction and oil swelling, and CO_2 had the highest diffusion coefficient. From these results, ethane and CO_2 are appropriate solvents for this crude oil. (3) The solubility of the solvent, especially for vaporized solvents, is an essential factor for investigation of the effective EOR processes. (4) Isomers can have different influences on the oil viscosity, even though their molecular properties are very similar. Such information will be used for further development of the digital oil model. In the current work, we combined a PVT simulator and MD simulations to study the live oil properties. In future, it will be interesting to perform large-scale MD

simulations,[24] such as with coarse-grained digital oil models, to identify the liquid phase components using molecular models.

AUTHOR INFORMATION

Corresponding Authors

*E-mail: liang@sys.t.u-tokyo.ac.jp; liang@race.u-tokyo.ac.jp (Y. L.)

*E-mail: masuda.yoshi@sys.t.u-tokyo.ac.jp (Y. M.)

ORCID

Yunfeng Liang: 0000-0002-8832-1778

Masato Morimoto: 0000-0003-3659-7913

Notes

The authors declare no competing financial interest.

ACKNOWLEDGMENTS

The authors thank the Japan Society for the Promotion of Science (JSPS) for a Grant-in-Aid for Scientific Research A (No. 24246148) and Grants-in-Aid for Scientific Research C (Nos. 16K06925 and 17K06988). We also acknowledge funding from Japan Petroleum Exploration Co., Ltd. (JAPEX). We would also like to thank Dr. Shinya Sato of AIST, Mrs. Hironori Imazato, Masanori Nakano, Hideyuki Nakashima, and Ryo Ueda of JAPEX, and Mr. Jo Mizuhara at the University of Tokyo for technical support and insightful comments.

REFERENCES

(1) Curtis C.; *et al.* Heavy-Oil Reservoirs. *Oilfield Review* **2002**, *14*, 30–51.

(2) Alboudwarej, H.; *et al.* Highlighting Heavy Oil. *Oilfield Review* **2006**, *18*, 34–53.

(3) Gray, M. R. *Upgrading Petroleum Residues and Heavy Oils*; Marcel Dekker: New York, 1994.

(4) Mullins, O. C. *Petroleomics and Structure-Function Relations of Crude Oils and Asphaltenes. Asphaltenes, Heavy Oils, and Petroleomics*; Mullins, O.C.; Sheu, E.Y.; Hammami, A.; Marshall, A.G., Eds.; Springer: New York, 2007, pp.1–16.

(5) Mohammadzadeh, O.; Rezaei, N.; Chatzis, I. Production Characteristics of the Steam-Assisted Gravity Drainage (SAGD) and Solvent-Aided SAGD (SA-SAGD) Processes Using a 2-D Macroscale Physical Model. *Energy Fuels* **2012**, *26*, 4346–4365.

(6) Keshavarz, M.; Okuno, R.; Babadagli, T. Efficient Oil Displacement Near the Chamber Edge in ES-SAGD. *J. Pet. Sci. Eng.* **2014**, *118*, 99–113.

(7) Keshavarz, M.; Okuno, R.; Babadagli, T. A Semi-Analytical Solution to Optimize Single-Component Solvent Coinjection with Steam during SAGD. *Fuel* **2015**, *144*, 400–414.

(8) Imai, M.; Mikami, K.; Suganuma, T.; Tsuchiya, Y.; Nakagawa, K.; Takahashi, S. Determination of Binary Diffusion Coefficients between Hot Liquid Solvents and Bitumen with X-ray CT. *J. Petrol. Sci. Eng.* **2019**, *177*, 496–507.

(9) Zborowski, M.; Writer, T. New Oil Sands Development Gets Green Light. J. Petrol. Tech. **2019**, *71*, 20–22.

(10) Butler, R. M.; Mokrys, I. J. A New Process (VAPEX) for Recovering Heavy Oils Using Hot Water and Hydrocarbon Vapour. *J. Can. Pet. Technol.* **1991**, *30*, 97–105.

(11) Das, S. K.; Butler, R. M. Diffusion Coefficients of Propane and Butane in Peace River

Bitumen. *Can. J. Chem. Eng.* **1996**, *74*, 985–992.

(12) Upreti, S. R.; Lohi, A.; Kapadia, R. A.; El-Haj, R. Vapor Extraction of Heavy Oil and Bitumen: A Review. *Energy Fuels* **2007**, *21*, 1562–1574.

(13) Torabi, F.; Yadali Jamaloei, B.; Stengler, B. M.; Jackson, D. E. The Evaluation of CO_2-Based Vapour Extraction (VAPEX) process for Heavy-Oil Recovery. *J. Pet. Explor. Prod. Technol.* **2012**, *2*, 93–105.

(14) Yang, C.; Gu, Y. Diffusion Coefficients and Oil Swelling Factors of Carbon Dioxide, Methane, Ethane, Propane, and Their Mixtures in Heavy Oil. *Fluid Phase Equilib.* **2006**, *243*, 64–73.

(15) Ohata, T.; Nakano, M.; Ueda, R. Evaluation of Molecular Diffusion Effect by Using PVT Experimental Data: Impact on Gas Injection to Tight Fractured Gas Condensate / Heavy Oil Reservoirs. *SPE Asia Pacific Unconventional Resources Conference and Exhibition, Brisbane, Australia, 9–11 November, 2015*, SPE-176968-MS.

(16) Kim, T. H.; Cho, J.; Lee, K. S. Modeling of CO_2 Flooding and Huff and Puff Considering Molecular Diffusion and Stress-Dependent Deformation in Tight Oil Reservoir. *SPE Europec featured at 79th EAGE Conference and Exhibition, Paris, France, 12–15 June, 2017*, SPE-185783-MS.

(17) Mulliken, C. A.; Sandler, S. I. The Prediction of CO_2 Solubility and Swelling Factors for Enhanced Oil Recovery. *Ind. Eng. Chem. Process Des. Dev.* **1980**, *19*, 709–711.

(18) van Buuren, A.; Marrink, S.; Berendsen, H. A Molecular-Dynamics Study of the Decane Water Interface. *J. Phys. Chem.* **1993**, *97*, 9206–9212.

(19) Bresme, F.; Chacon, E.; Tarazona, P.; Tay, K. Intrinsic Structure of Hydrophobic Surfaces: The Oil-Water Interfaces. *Phys. Rev. Lett.* **2008**, *101*, 056102.

(20) Jang, S. S.; Lin, S.-T.; Maiti, P. K.; Blanco, M.; Goddard, W. A., III. Molecular Dynamics Study of a Surfactant-Mediated Decane-Water Interface: Effect of Molecular Architecture of Alkyl Benzene Sulfonate. *J. Phys. Chem. B* **2004**, *108*, 12130–12140.

(21) Kunieda, M.; Nakaoka, K.; Liang, Y.; Miranda, C. R.; Ueda, A.; Takahashi, S.; Okabe, H.; Matsuoka, T. Self-Accumulation of Aromatics at the Oil-Water Interface through Weak Hydrogen Bonding. *J. Am. Chem. Soc.* **2010**, *132*, 18281–18286.

(22) Makimura, D.; Kunieda, M.; Liang, Y.; Matsuoka, T.; Takahashi, S.; Okabe, H. Application of Molecular Simulations to CO_2-Enhanced Oil Recovery: Phase Equilibrium and Interfacial Phenomena. *SPE Journal* **2012**, *18*, 319–330.

(23) Mikami, Y.; Liang, Y.; Matsuoka, T.; Boek, E. S. Molecular Dynamics Simulations of Asphaltenes at the Oil-Water Interface: From Nanoaggregation to Thin-Film Formation. *Energy Fuels* **2013**, *27*, 1838–1845.

(24) Herdes, C.; Totton, T. S.; Muller, E. A. Coarse Grained Force Field for the Molecular Simulation of Natural Gases and Condensates. *Fluid Phase Equilib.* **2015**, *406*, 91–100.

(25) Castellano, O.; Gimon, R.; Canelon, C.; Aray, Y.; Soscun, H. Molecular Interactions between Orinoco Belt Resins. *Energy Fuels* **2012**, *26*, 2711–2720.

(26) Silva, H. S.; Sodero, A. C. R.; Bouyssiere, B.; Carrier, H.; Korb, J. -P.; Alfarra, A.; Vallverdu, G.; Bégué, D.; Baraille, I. Molecular Dynamics Study of Nanoaggregation in Asphaltene Mixtures: Effects of the N, O, and S Heteroatoms. *Energy Fuels* **2016**, *30*, 5656–5664.

(27) Aquing, M.; Ciotta, F.; Creton, B.; Fejéan, C.; Pina, A.; Dartiguelongue, C.; Trusler, J. P. M.; Vignais, R.; Lugo, R.; Ungerer, P.; Nieto-Draghi, C. Composition Analysis and Viscosity Prediction of Complex Fuel Mixtures Using a Molecular-Based Approach. *Energy*

Fuels **2012**, *26*, 2220–2230.

(28) Zhang, L.; Greenfield, M. L. Relaxation Time, Diffusion, and Viscosity Analysis of Model Asphalt Systems using Molecular Simulation. *J. Chem. Phys.* **2007**, *127*, 194502.

(29) Zhang, L.; Greenfield, M. L. Analyzing Properties of Model Asphalts Using Molecular Simulation. *Energy Fuels* **2007**, *21*, 1712–1716.

(30) Li, D. D.; Greenfield, M. L. Chemical Compositions of Improved Model Asphalt Systems for Molecular Simulations. *Fuel* **2014**, *115*, 347–356.

(31) Sheremata, J. M.; Gray, M. R.; Dettman, H. D.; McCaffrey, W. C. Quantitative Molecular Representation and Sequential Optimization of Athabasca Asphaltenes. *Energy Fuels* **2004**, *18*, 1377–1384.

(32) Boek, E. S.; Yakovlev, D. S.; Headen, T. F. Quantitative Molecular Representation of Asphaltenes and Molecular Dynamics Simulation of Their Aggregation. *Energy Fuels* **2009,** *23*, 1209–1219.

(33) Sugiyama, S.; Liang, Y.; Murata, S.; Matsuoka, T.; Morimoto, M.; Ohata, T.; Nakano, M.; Boek, E. S. Construction, Validation, and Application of Digital Oil: Investigation of Asphaltene Association Toward Asphaltene-Precipitation Prediction. *SPE Journal* **2018**, *23*, 952–968, SPE-189465-PA.

(34) Iwase, M; Sugiyama, S.; Liang, Y.; Masuda, Y.; Morimoto, M.; Matsuoka, T.; Boek, E. S.; Ueda, R.; Nakagawa, K. Development of Digital Oil for Heavy Crude Oil: Molecular Model and Molecular Dynamics Simulations. *Energy Fuels* **2018**, *32*, 2781–2792.

(35) Abraham, M. J.; Murtola, T.; Schulz, R.; Pall, S.; Smith, J. C.; Hess, B.; Lindah, E. GROMACS: High Performance Molecular Simulations through Multi-Level Parallelism from Laptops to Supercomputers. *SoftwareX* **2015**, *1–2*, 19–25.

(36) Vanommeslaeghe, K.; Hatcher, E.; Acharya, C.; Kundu, S.; Zhong, S.; Shim, J.; Darian, E.; Guvench, O.; Lopes, P.; Vorobyov, I.; MacKerell, A. D., Jr. CHARMM General Force Field: A Force Field for Drug-Like Molecules Compatible with the CHARMM All-Atom Additive Biological Force Fields. *J. Comput. Chem*. **2010**, *31*, 671–690.

(37) Vanommeslaeghe, K.; MacKerell, A. D., Jr. Automation of the CHARMM General Force Field (CGenFF) 1: Bond Perception and Atom Typing. *J. Chem. Inf. Model*. **2012**, *52*, 3144–3154.

(38) Vanommeslaeghe, K.; Raman, E. P.; MacKerell, A. D., Jr. Automation of the CHARMM General Force Field (CGenFF) 2: Assignment of Bonded Parameters and Partial Atomic Charges. *J. Chem. Inf. Model*. **2012**, *52*, 3155–3168.

(39) Yu, W.; He, X.; Vanommeslaeghe, K.; MacKerell, A. D., Jr. Extension of the CHARMM General Force Field to Sulfonyl-Containing Compounds and Its Utility in Biomolecular Simulation. *J. Comput. Chem*. **2012**, *33*, 2451–2468.

(40) Caleman, C.; van Maaren, P. J.; Hong, M.; Hub, J. S.; Costa, L. T.; van der Spoel, D. Force Field Benchmark of Organic Liquids: Density, Enthalpy of Vaporization, Heat Capacities, Surface Tension, Isothermal Compressibility, Volumetric Expansion Coefficient, and Dielectric Constant. *J. Chem. Theory Comput.* **2012**, *8*, 61–74.

(41) Potoff, J. J.; Siepmann, J. I. Vapor–liquid equilibria of mixtures containing alkanes, carbon dioxide, and nitrogen. *AIChE J.* **2001**, 47, 1676–1682.

(42) Pall, S.; Hess, B. A Flexible Algorithm for Calculating Pair Interactions on SIMD Architectures. *Comput. Phys. Commun.* **2013**, *184*, 2641–2650.

(43) Essmann, U.; Perera, L.; Berkowitz, M. L.; Darden, T.; Lee, H.; Pedersen, L. G. A Smooth Particle Mesh Ewald Method. *J. Chem. Phys*. **1995**, *103*, 8577–8593.

(44) Bussi, G.; Donadio, D.; Parrinello, M. Canonical Sampling through Velocity Rescaling. *J. Chem. Phys.* **2007**, *126*, 014101.

(45) Berendsen, H. J. C.; Postma, J. P. M.; van Gunsteren, W. F.; DiNola, A.; Haak, J. R. Molecular Dynamics with Coupling to an External Bath. *J. Chem. Phys.* **1984**, *81*, 3684–3690.

(46) Nosé, S. A molecular Dynamics Method for Simulations in the Canonical Ensemble. *Mol. Phys.* **1984**, *52*, 255–268.

(47) Hoover, W. G. Canonical Dynamics: Equilibrium Phase-Space Distributions. *Phys. Rev. A: At., Mol., Opt. Phys.* **1985**, *31*, 1695–1697.

(48) Parrinello, M.; Rahman, A. Strain Fluctuations and Elastic Constants. *J. Chem. Phys.* **1982**, *76*, 2662–2666.

(49) Chen, T.; Smit, B.; Bell, A. T. Are Pressure Fluctuation-Based Equilibrium Methods Really Worse than Nonequilibrium Methods for Calculating Viscosities? *J. Chem. Phys.* **2009**, *131*, 246101.

(50) Pedersen, K. S.; Milter, J.; Sorensen, H. Cubic Equations of State Applied to HT/HP and Highly Aromatic Fluids. *SPE Journal* **2004**, *10*,186–192.

(51) Williams, G.; Watts, D. C.; Dev, S. B.; North, A.M. Further Considerations of Non-Symmetrical Dielectric Relaxation Behavior Arising from a Simple Empirical Decay Function. *Trans. Faraday Soc.* **1971**; 67, 1323–1335.

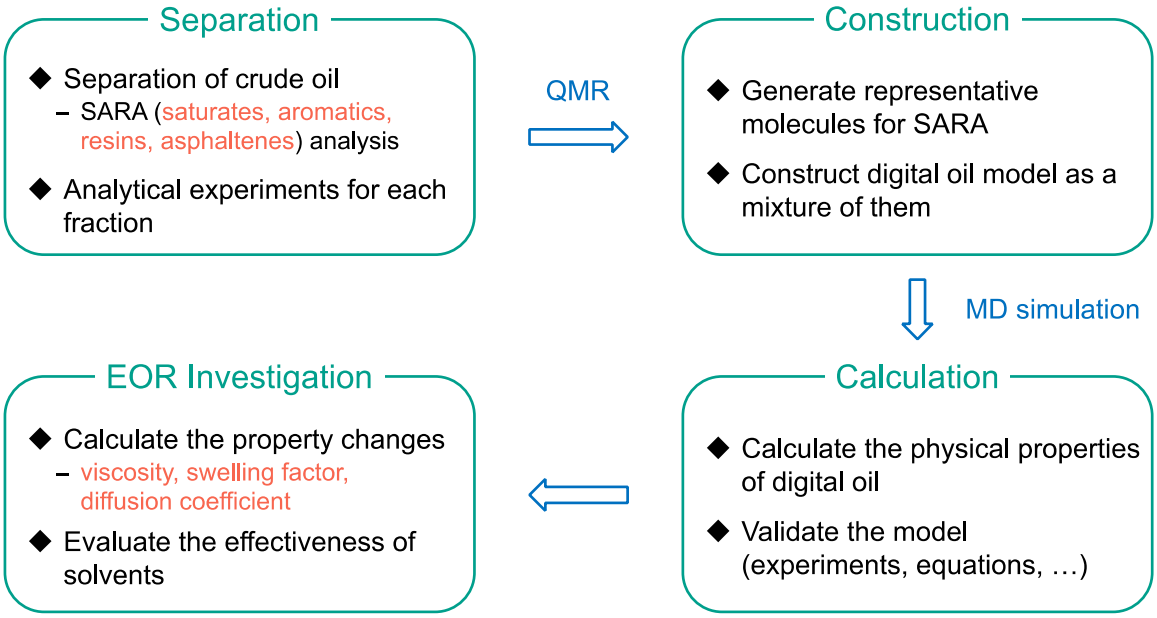

Figure 1. Schematic diagram of the solvent based EOR study with digital oil.

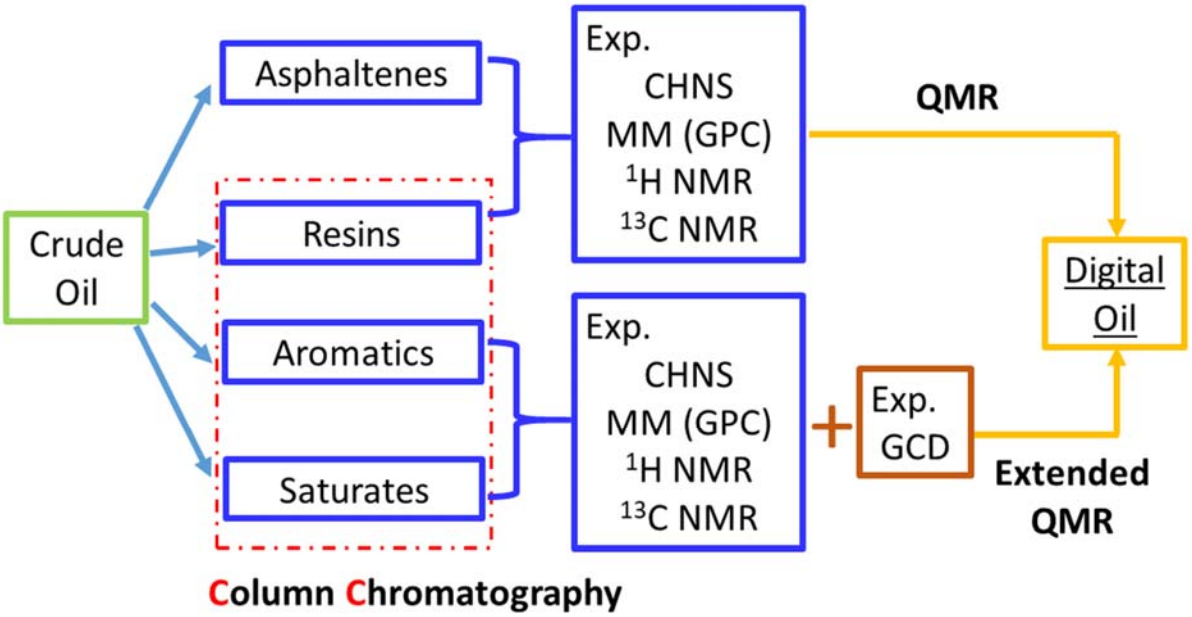

Figure 2. Construction of a digital oil model for a heavy crude oil. This diagram was constructed based on the procedure described in Ref. [34]. Note that CHNS means elemental analysis, MM (GPC) means molecular mass measurement by gel permeation chromatography, ^{1}H and ^{13}C NMR spectroscopy reveal the structural types of hydrogen and carbon atoms, QMR represents the quantitative molecular representation based on the average data (e.g., the average molecular mass), and extended QMR considers the mass distribution resulting from GCD experiments. Extended QMR can generate molecular structures without aromatic rings. The lost components were determined based on GCD experiments.

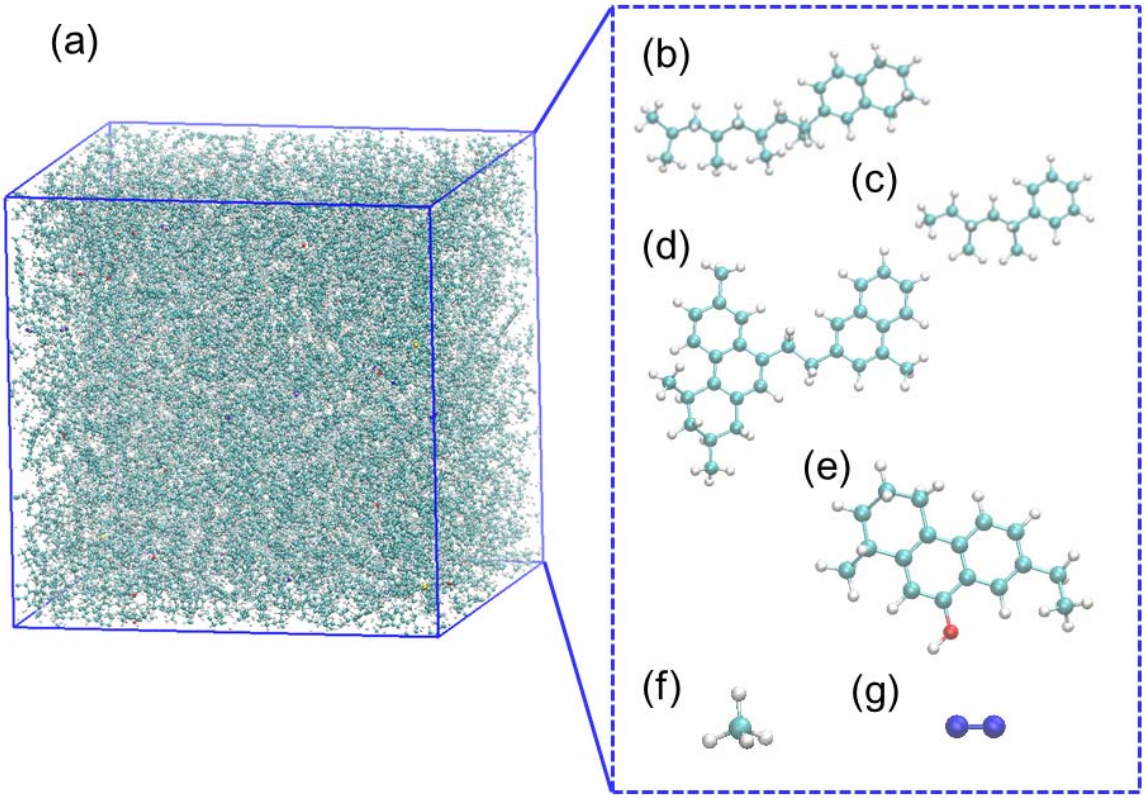

Figure 3. Snapshot of the digital oil at 24.2 MPa and 325.15 K (a). The insert shows the representative molecules with the highest mole percentage for saturates (b), lost components (c), aromatics (d), resins (e), and dissolved gases CH_4 (f) and N_2 (g). The mole fraction breakdown is given in **Table 1**. After equilibrium, the simulation box had dimensions of ~7.75 nm × 7.75 nm × 7.75 nm.

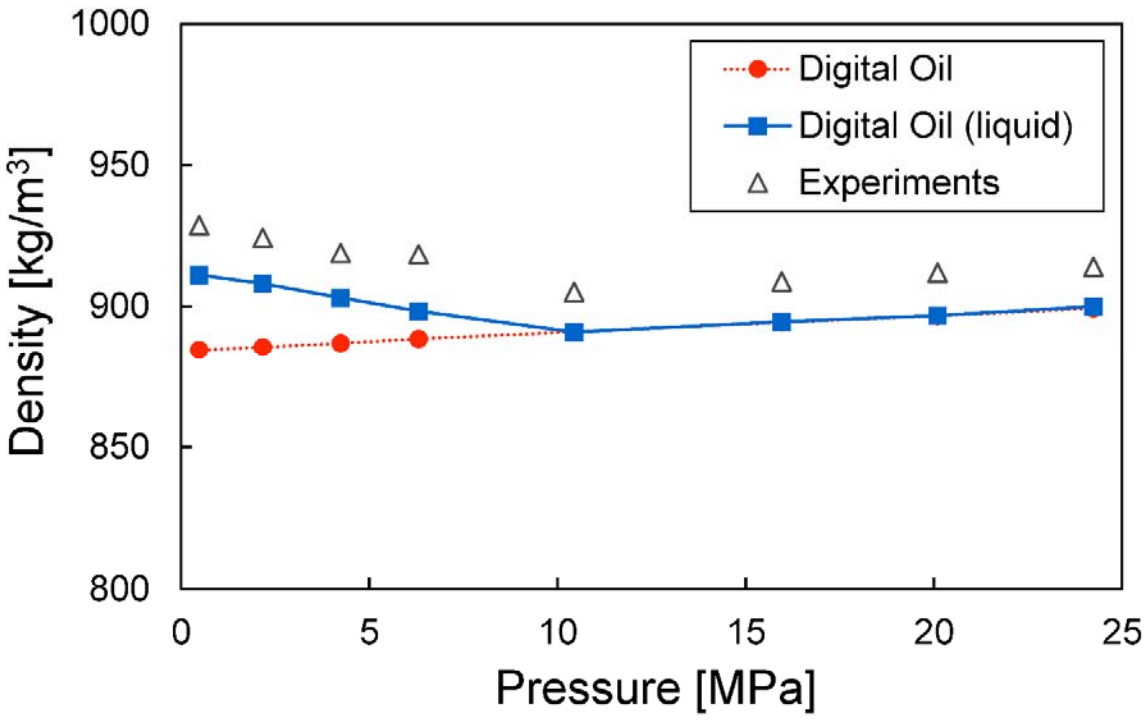

Figure 4. Densities calculated using the full components of the digital oil and the liquid phase of the digital oil and the experimentally measured values at different pressures.

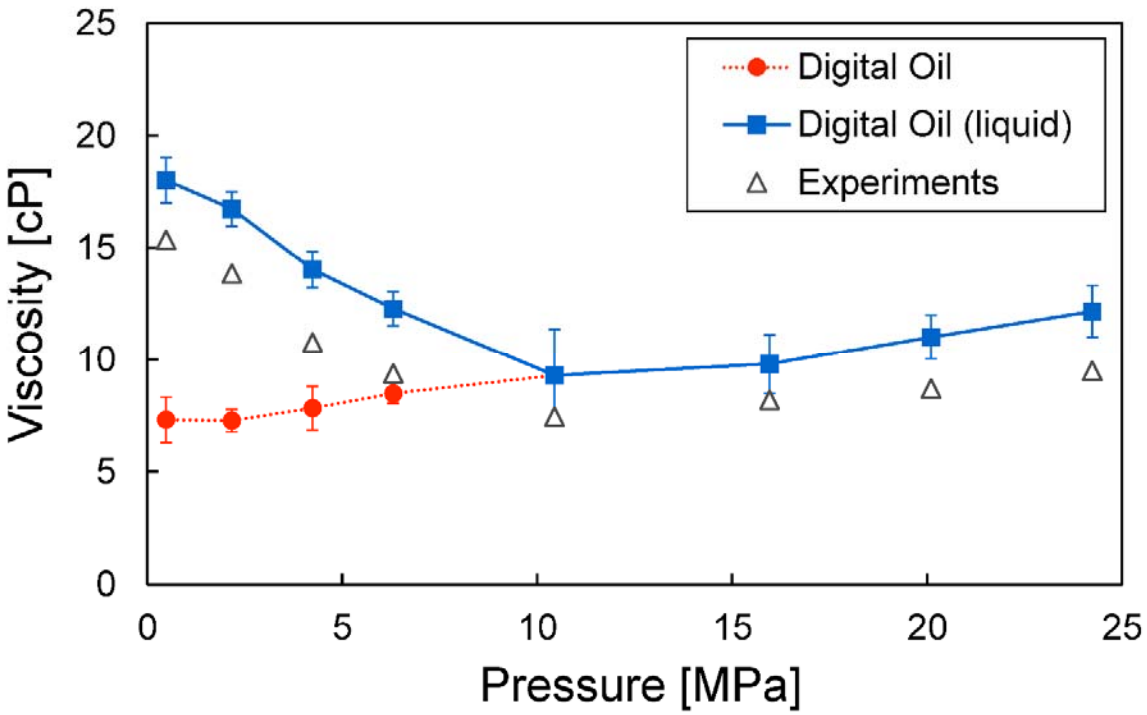

Figure 5. Calculated viscosities using the full components of the digital oil and the liquid phase of the digital oil and the experimentally measured values at different pressures.

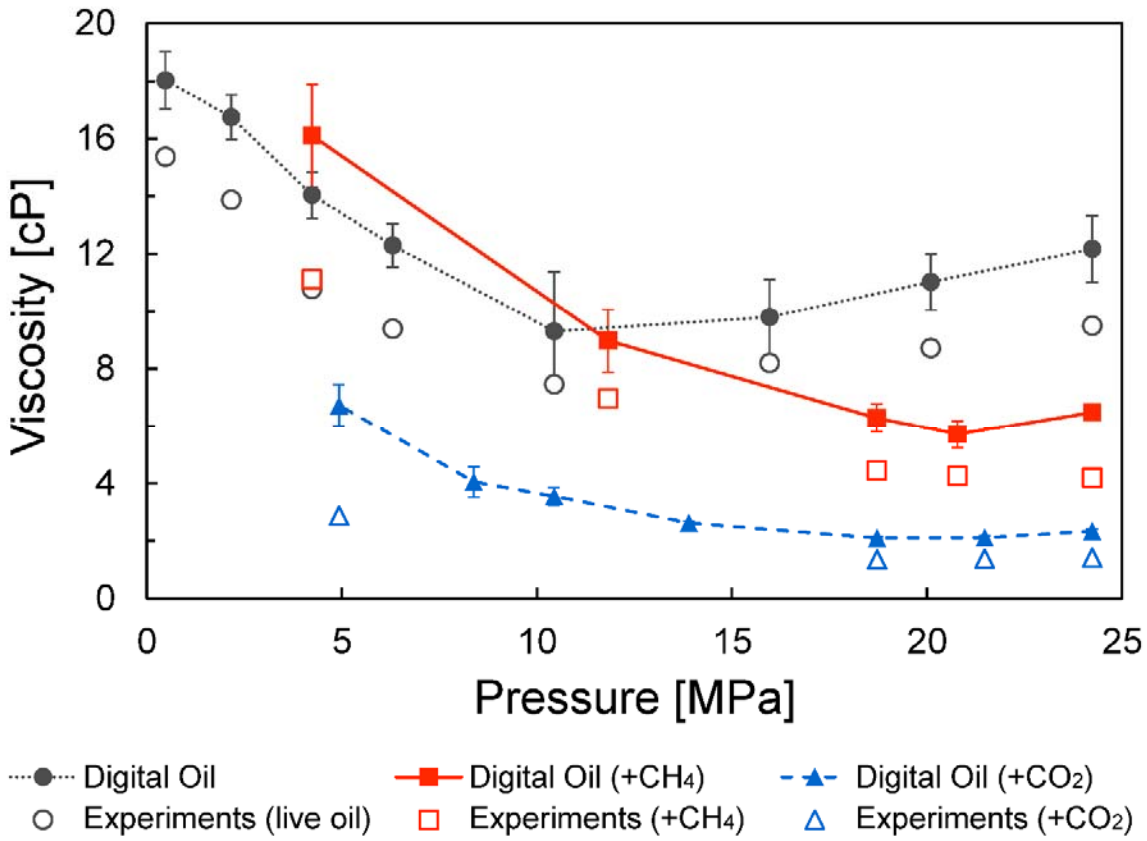

Figure 6. Calculated viscosities of the digital oil, digital oil–CH_4 mixture, and digital oil–CO_2 mixture in comparison with the experimentally measured values.

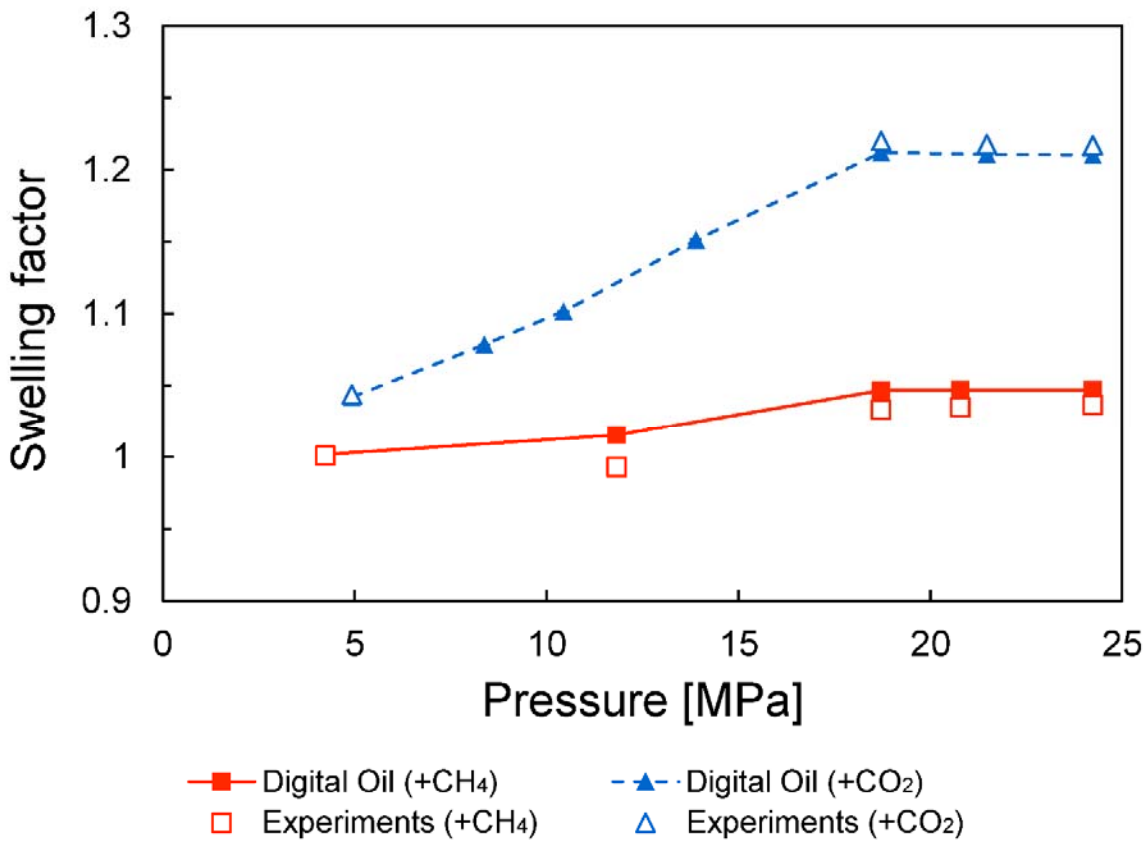

Figure 7. Calculated swelling factors of the digital oil, digital oil–CH_4 mixture, and digital oil–CO_2 mixture in comparison with the experimentally measured values. Note that both the experimental and calculated swelling factors were derived based on the density ratio.

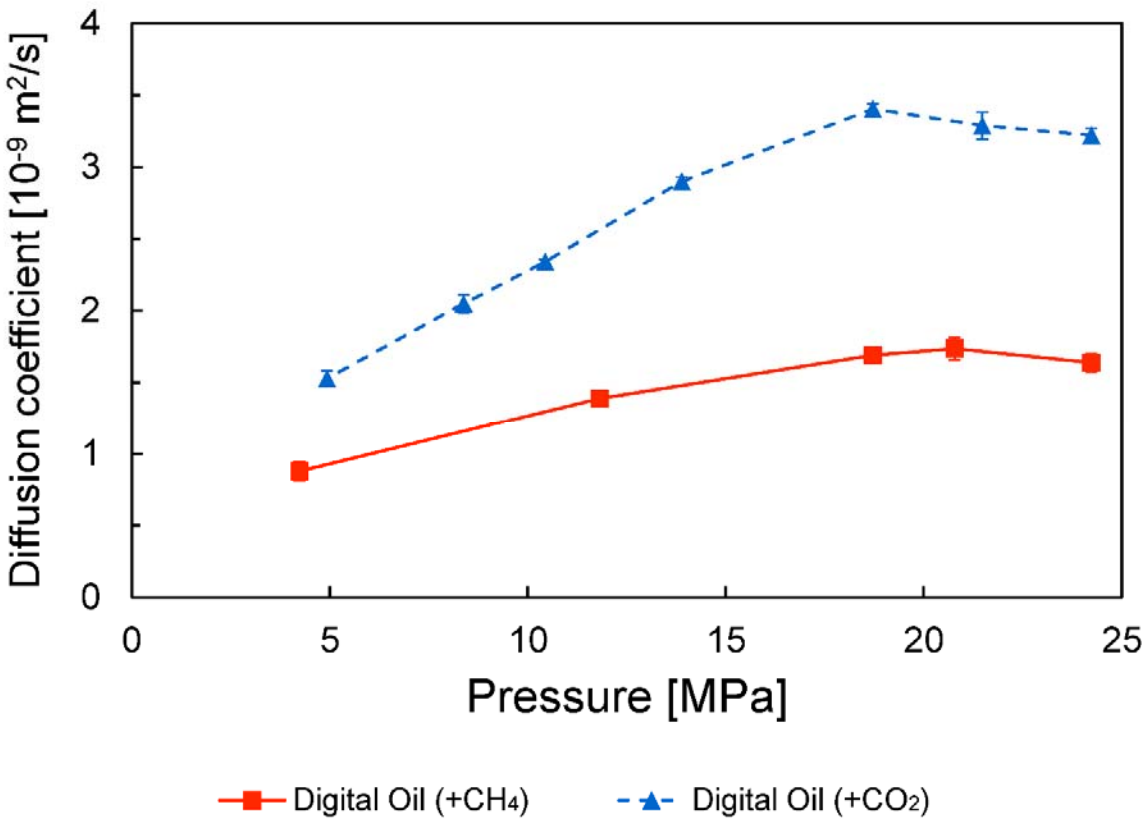

Figure 8. Calculated diffusion coefficients of CH_4 and CO_2 in the digital oil.

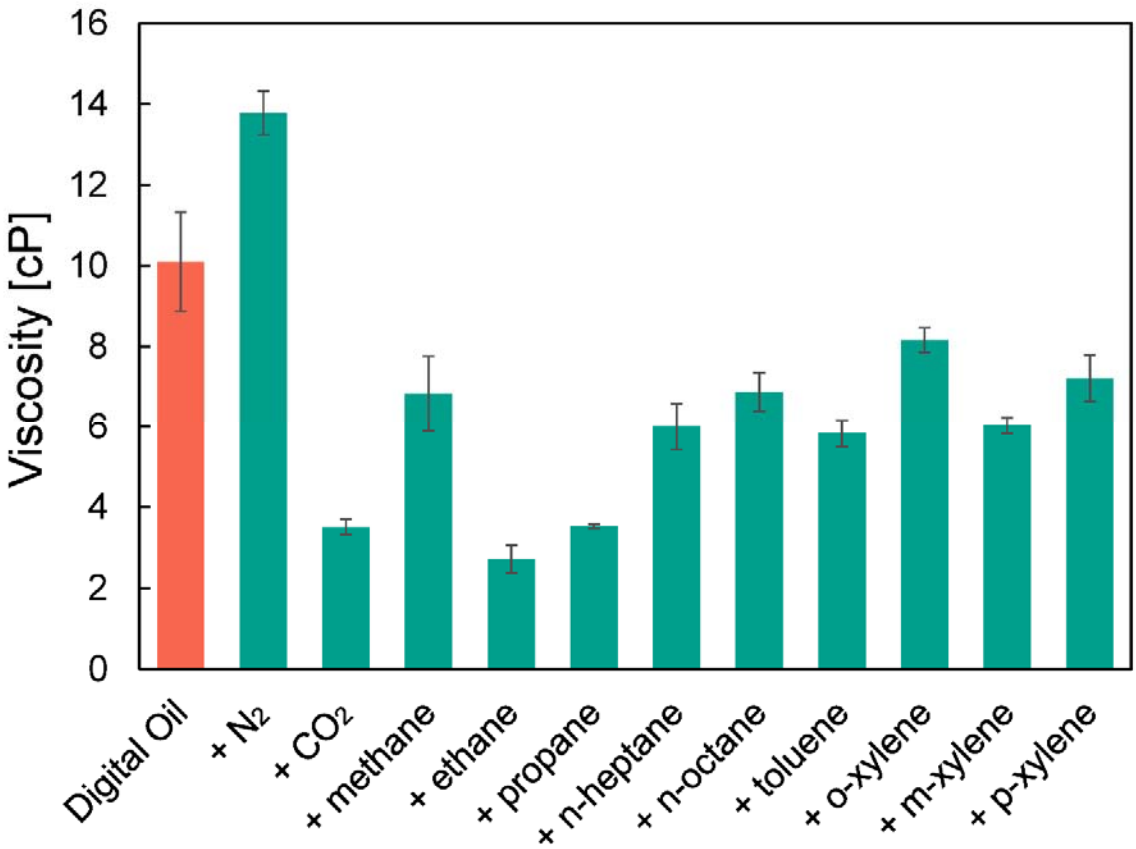

Figure 9. Comparison of the calculated viscosities of the digital oil on adding different solvents. The green bar is the viscosity on adding each solvent. The orange bar is the original viscosity of the digital oil alone.

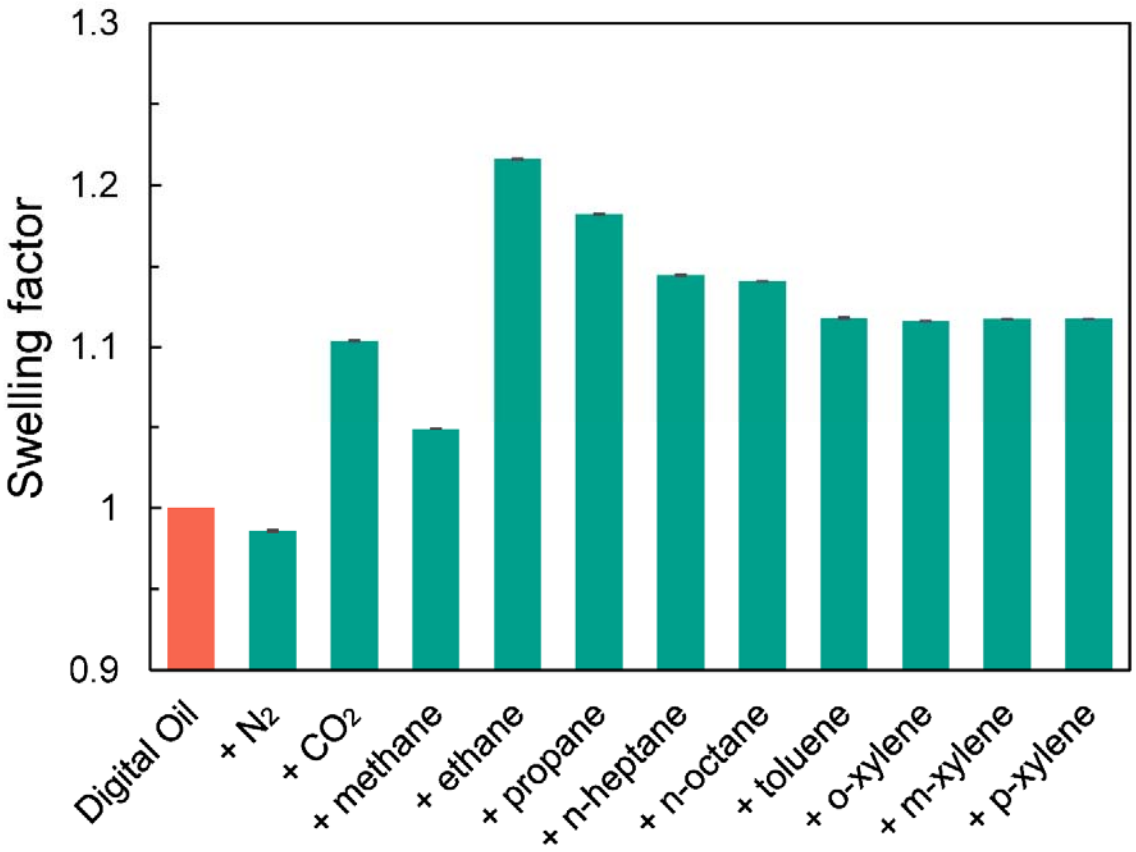

Figure 10. Comparison of the swelling factors of the digital oil on adding different solvents. The green bar is the swelling factor on adding each solvent. The orange bar is the original volume of the digital oil alone.

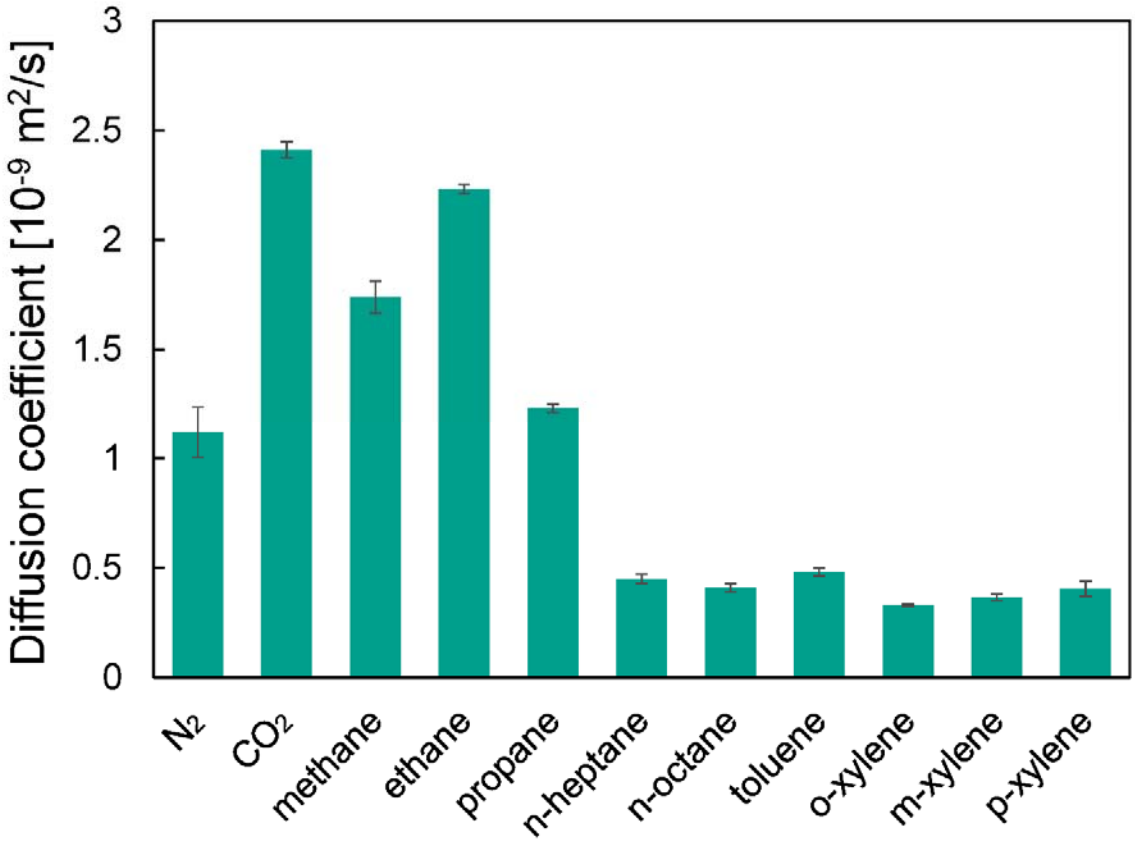

Figure 11. Comparison of the diffusion coefficients of different solvents in the digital oil.

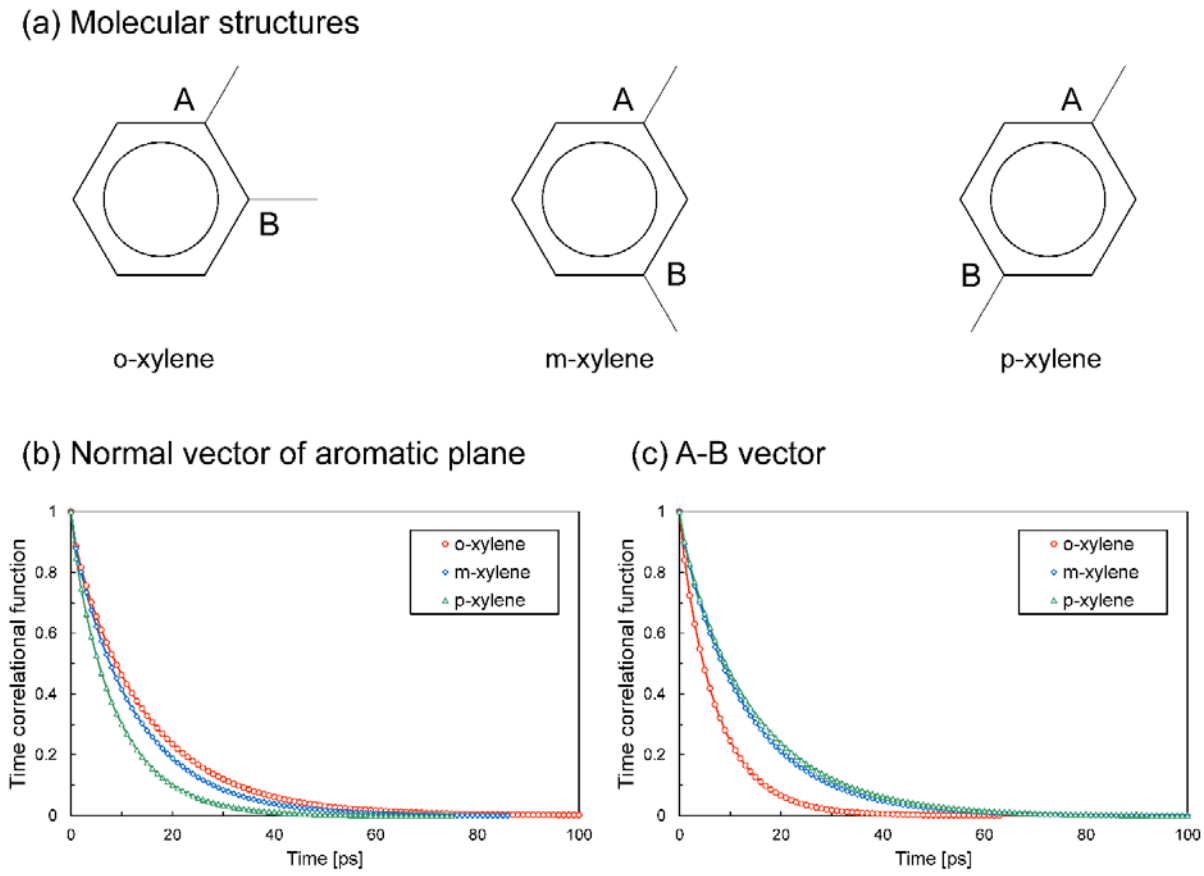

Figure 12. (a) Molecular structures of the xylene isomers, (b) time correlation function of the normal vector of the aromatic plane, and (c) time correlation function of the A–B vector in the aromatic plane. The A and B atoms used in each xylene isomer are labeled in (a).

Table 1. Yields of the SARA fractions in the crude oil sample

Fraction	Saturates	Aromatics	Resins	Asphaltenes	Lost components
Yield (wt %)	41.1	16.1	3.0	0.4	39.4

Table 2. Mole fraction and number of molecules of the gas components in the live oil model

Component	mol %	Number of molecules
N_2	1.06	13
CO_2	0.04	0
C_1	23.03	279
C_2	0.05	0
C_3	0.00	0
C_{7+} (dead oil)	75.82	917

Table 3. Composition of the liquid phase of the live oil model at each pressure

	Number of molecules in liquid phase				
	Pressure [MPa]				
	P>9.84	6.31	4.24	2.17	0.48
N_2	13	5	2	0	0
C_1	279	183	126	66	15
C_{7+} (dead oil)	917	917	917	917	917

Table 4. Composition of the liquid phase of the live oil model at each pressure on adding CH_4

	Number of molecules in liquid phase		
	Pressure (MPa)		
	P>17.18	11.82	4.24
N_2	13	6	1
C_1	557	375	133
C_{7+} (dead oil)	917	917	917

Table 5. Composition of the liquid phase of the live oil model at each pressure on adding CO_2

	Number of molecules in liquid phase				
	Pressure [MPa]				
	P>18.45	13.89	10.44	8.38	4.93
N_2	1	1	0	0	0
CO_2	1363	1048	802	641	368
C_1	215	166	111	77	31
C_{7+} (dead oil)	917	917	917	917	917

Table 6. Number of molecules of each solvent added to the digital oil

Solvent	Molecular mass	Number of molecules
N_2	28	998
CO_2	44	635
methane	16	1746
ethane	30	931
propane	44	635
n-heptane	100	279
n-octane	114	245
toluene	92	304
o-xylene	106	264
m-xylene	106	264
p-xylene	106	264

Table 7. Compositions of the liquid phases of the digital oil–N_2 and digital oil–methane mixtures

	Number of molecules	
	Solvent	
	N_2	methane
N_2	122	2
C_1	81	574
C_{7+} (dead oil)	917	917

Table 8. Xylene rotational relaxation times and the regression results using the modified Kohlrausch–Williams–Watts function[51]

	Normal vector of aromatic plane				
	α	β	τ_0	τ_{KWW}	Integration (τ_C)
o-xylene	0.89	0.58	14.9	2.02	13.6
m-xylene	0.91	0.65	12.6	1.40	11.7
p-xylene	0.87	0.64	9.21	1.96	8.39
	A-B vector				
	α	β	τ_0	τ_{KWW}	Integration (τ_C)
o-xylene	0.86	0.70	7.65	2.83	7.12
m-xylene	0.91	0.62	13.5	2.45	12.7
p-xylene	0.90	0.73	15.0	2.43	13.9